energies

MDPI

Article

Theoretical and Experimental Investigation on Thermal Characteristics of Railway Double-Row Tapered Roller Bearing

Pengfei Gao, Wuchu Tang, Yunxian Cui, Yuchen Wang, Guowei Mo and Junwei Yin *

School of Mechanical Engineering, Dalian Jiaotong University, Dalian 116028, China; gaopengfei198935@163.com (P.G.); tangwuchu@126.com (W.T.); dlcyx007@126.com (Y.C.); hqdishrua@gmail.com (Y.W.); moguowei00@163.com (G.M.)
* Correspondence: yjwzx@djtu.edu.cn

Abstract: The research on the thermal characteristics of railway double-row tapered roller bearing is of great significance for its structural design and operation monitoring. We established the quasi-static mechanical model of the bearing according to the test conditions, and we obtained the load distribution and kinematic parameters of the bearing. We studied the temperature distribution of railway double-row tapered roller bearing under test conditions through finite element analysis, which was consistent with the test results. We built a bearing testbed to study the effects of different rotating speeds on the temperature distribution of the bearing inner ring, outer ring, and roller. The results show that the speed dramatically affects the bearing inner ring. With the rate increase, the temperature difference between the inner and outer rings decreases gradually, and the temperature at the large end of the roller is the highest.

Keywords: railway bearing; adaptive thin-film temperature sensor; temperature distribution; circumferential temperature; radial temperature; axial temperature

Citation: Gao, P.; Tang, W.; Cui, Y.; Wang, Y.; Mo, G.; Yin, J. Theoretical and Experimental Investigation on Thermal Characteristics of Railway Double-Row Tapered Roller Bearing. *Energies* **2022**, *15*, 4217. https://doi.org/10.3390/en15124217

Academic Editor: Gabriela Huminic

Received: 6 May 2022
Accepted: 6 June 2022
Published: 8 June 2022

1. Introduction

The railway bearing studied in this paper is a double-row tapered roller bearing, which is mainly used to carry and transmit motion. When the train is running, the internal friction of the railway bearing is constant, of which the most prominent feature is the temperature rise in various parts in the bearing. If the heat increases rapidly due to some odd reason, it may lead to bearing overheating [1,2]. It may change the internal lubrication of the bearing and the working clearance between parts, and even deform the bearing. It may also increase local stress and local temperature in the bearing, accelerate the wear of the bearing, shorten the service life of the bearing [3,4], and even lead to early scrapping of bearing components, such as burning and jamming [5]. Especially when the train passes a curve, the load carried by the left and right trains of railway bearings is inconsistent, and the friction heat and temperature distribution of bearings are more complex. Therefore, studying the temperature rise and diffusion of bearings is essential, which can provide theoretical and technical guidance for the research and localization of railway bearings.

There is much research on the heat generation mechanism, and temperature field of double-row tapered roller bearings. Early researchers mainly monitored several points in the experimental study due to sensor size and installation space limitations, such as the bearing seat or bearing outer ring. For example, Winer [6] created a heat source to simulate the heating process of the bearings, using infrared scanners and thermocouples to record the outer ring temperature of bearings. Hoeprich [7] used thermocouples and thermal coatings to obtain the outer bearing ring and inner ring temperatures. Craig [8] used thermocouple sensors to monitor the bearing oil inlet and outer ring temperature to reflect the bearing status. With the increasing speed of the train, the temperature measurement of railway bearing has attracted more and more attention. Takabi [9] installed standard K-type thermocouples on the bearing to obtain outer ring temperature and lubricate oil

temperature. Jeng [10] installed resistance temperature sensors on the bearing pedestal to study the laws of bearing temperature affected by oil volume, preload, airflow, and speed. Jiang [11] studied the effects of oil pipe length, nozzle, lubrication interval, oil viscosity, and oil type on bearing temperature rise, providing different ideas for studying bearing temperature. Li [12] used PT100 platinum resistance to measure the single point temperature of the conical bearing outer ring and studied the influence of axial preload and oil supply pressure on it. These temperature measuring points are far away from the friction parts or damaged parts of the bearing, which will cause some significant delays and errors in the measurement results [13]. To further study the bearing temperature field, scholars began to explore multi-point temperature measurement methods and temperature measurement of rotating parts. Tarawneh [14] used a heater to heat two rollers to study the heat transfer path of railway tapered roller bearings under a static state. Subsequently, Tarawneh [15] evenly arranged six temperature sensors along the outer ring of the bearing to detect the circumferential temperature of the bearing surface. Flouros [16] fixed the infrared detector on the bearing seat and recorded the surface temperature of the inner ring during the rotation of the bearing. Dong [17] and Liu [18] conducted experiments with fiber Bragg grating sensors and studied the temperature distribution of the outer ring of the bearing. Henao-Sepulveda [19] developed a radio frequency-based wireless digital transmission method to realize the complex problem bearing cage temperature measurements. Brecher [20] developed a telemetry system to measure the temperature of the inner ring with PT-100 temperature sensors. The system uses infrared temperature measurement technology and wireless transmission technology, and the poor working environment of the bearing affects the stability of the signal transmission. Zhou [21,22] built a multi-point temperature measurement test-bed to study the rotating speed and external load effects on the circumferential, axial, and radial temperature rise and temperature distribution of double-row tapered roller bearings. The results show that the temperature rise in the load zone of the outer bearing ring is high under a static load. Under the combined load, there are apparent temperature differences in the axial, circumferential, and radial directions of double-row tapered roller bearings. Yan et al. [23–25] developed the quantum dot temperature-sensitive sensor, gave full play to the temperature-sensitive fluorescence characteristics of the quantum dot material, coated it on the tested position, and solved the problem of temperature measurements of high-speed bearings. However, this method requires too many processes and can currently only be completed in the laboratory. Cui et al. [26] developed a thin-film thermocouple temperature sensor to measure the real-time temperature of bearing rollers during train operation. Its adaptive structure can maintain contact with the end face of the rolling element for measurement. The test results show that the roller temperature is 6~10 °C higher than the outer ring temperature.

2. Model and Simulation

2.1. Quasi Static Mechanical Model

According to the working conditions of the test bearing, we established the calculation model of roller contact load distribution under axial load only. Compared with the contact load between the roller and the inner and outer rings, there is little normal force between the roller and the cage pocket. We can ignore the tangential friction between the roller and the cage pocket in the calculation. The test bearing is shown in Figure 1 and F_a is the axial load.

As shown in Figure 2, for the stress analysis of the roller, the loads of the roller and the inner and outer raceways and the inner ring retaining edge are Q_i, Q_e and Q_f, respectively, and their contact angles are α_i, α_e and α_f. When the rollers are balanced, these loads must satisfy the following balance equations:

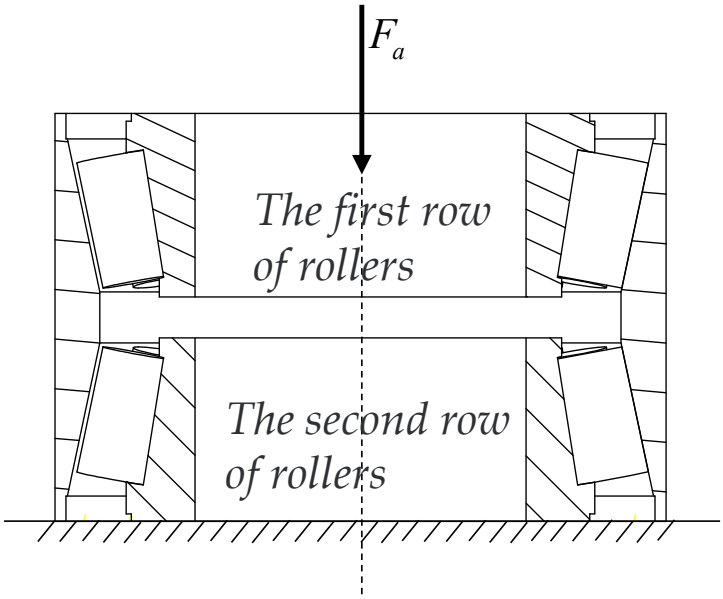

Figure 1. Test bearing.

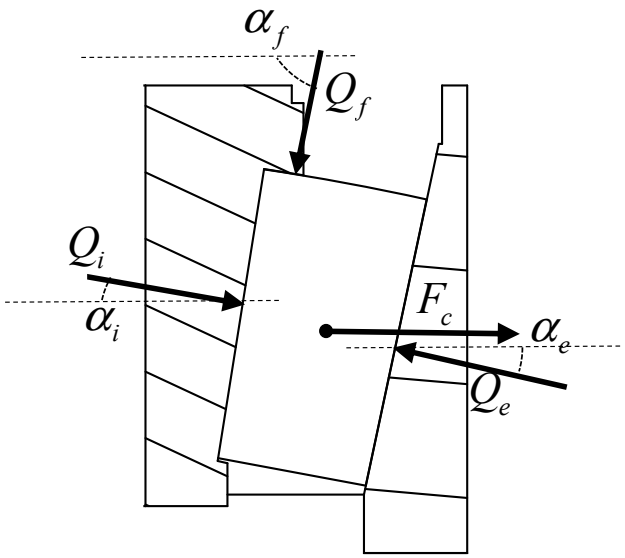

Figure 2. Stress analysis of roller.

Centrifugal force on rolling element F_c

$$F_c = 0.5 m d_m {w_c}^2 \tag{1}$$

$$Q_e \sin\alpha_e - Q_i \sin\alpha_i - Q_f \sin\alpha_f = 0 \tag{2}$$

$$Q_e \cos\alpha_e - Q_i \cos\alpha_i + Q_f \cos\alpha_f - F_c = 0 \tag{3}$$

The contact load Q_e of the outer raceway is the reference variable, which can be obtained from Equations (2)–(5).

$$Q_i = Q_e \frac{\sin(\alpha_e + \alpha_f)}{\sin(\alpha_i + \alpha_f)} - F_c \frac{\sin\alpha_f}{\sin(\alpha_i + \alpha_f)} = c_i Q_e - c_1 F_c \tag{4}$$

$$Q_f = Q_e \frac{\sin(\alpha_e - \alpha_i)}{\sin(\alpha_i + \alpha_f)} + F_c \frac{\sin\alpha_i}{\sin(\alpha_i + \alpha_f)} = c_f Q_e + c_2 F_c \tag{5}$$

As shown in Figure 3, under the action of axial load F_a, the bearing inner ring will produce axial displacement δ_a relative to the outer ring. For the ith roller, the total displacement along the contact normal direction of the outer raceway is as follows:

$$\delta_{ni} = \delta_a \sin \alpha_e \tag{6}$$

$$Q_{ei} = K_{ne} \delta_{ni}^{1.11} + F_c \cos \alpha_e \tag{7}$$

$$K_{ne} = 6.24 \times 10^4 l^{0.82} D_w^{0.11} \left[1 + c_i^{0.9} \cos(\alpha_e - \alpha_i)\right]^{-1.11} \tag{8}$$

where K_{ne} is the total stiffness coefficient at the contact of the outer raceway.

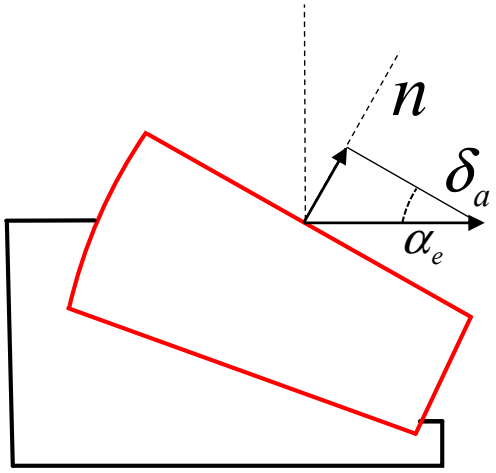

Figure 3. Displacement component.

The component of Q_{ei} in F_a direction is

$$Q_{ai} = Q_{ei} \sin \alpha_e \tag{9}$$

In this way, the balance equation of the bearing can be expressed as

$$F_a - \sum_{j=1}^{2} \sum_{i=1}^{Z} Q_{aji} = 0 \tag{10}$$

2.2. Heat Generation

Through the pseudo-static model of railway double-row tapered roller bearing, we calculated the tangential force and relative sliding speed between the roller and the inner and outer race raceways and between the roller and the inner race retaining edge, respectively. As shown in Figure 4, the product of force and speed is the friction heat of the bearing. When the bearing is running, the cage is suspended. The sliding friction loss between the roller and the cage accounts for a small proportion of the friction loss of the whole bearing, so we can ignore the role of the cage.

(1) Heat generation rate of sliding friction between roller and raceway

$$H_{RRCi(o)j} = \iint_S \tau \cdot \Delta V_{i(o)j} dxdy \tag{11}$$

where $\Delta V_{i(o)j}$ is the relative sliding speed between the jth roller and the inner (outer) raceway; τ is the shear stress in the contact area between the jth roller and the raceway.

(2) Friction rate between the sliding end of the roller and the inner ring

$$H_{REFj} = \mu_{fj} Q_{fj} \cdot \Delta V_{fj} \tag{12}$$

where Q_{fj} is the contact load between the large end of the jth roller and the retaining edge of the inner ring; ΔV_{fj} is the relative sliding rate between the jth roller and the inner ring flange; μ_{fj} is the friction coefficient between the large end of the jth roller and the retaining edge of the inner ring.

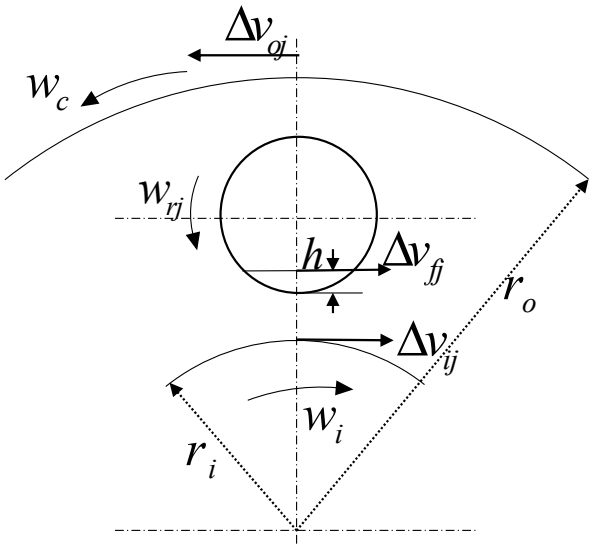

Figure 4. Movement relation.

(3) Viscous friction of lubricant

When the roller runs in the bearing cavity, it will be affected by the flow resistance of the grease gas mixture in the cavity, and the loss of flow resistance is

$$H_{fdrag} = 0.5 d_m F_V (w_m - w_o)^{0.81} \tag{13}$$

where F_V is the flow resistance around a single roller, $F_V = \frac{1}{8} C_d \rho D_W L (d_m w_m)^2$, D_W is the average diameter of the roller, d_m is the diameter of the bearing pitch circle, L is the effective length of the roller, and ρ is the density of the grease gas mixture in the bearing cavity; C_d is the resistance coefficient.

$C_d = 1.1642 - \frac{1.3796 R_e}{10^5 \ln(R_e)} + \frac{4.3388}{\sqrt{R_e}} + \frac{4.5113}{R_e}$ where R_e is the Reynolds number of the grease.

2.3. Heat Conduction

The heat generated in the working of the bearing is radiated outward through heat conduction, heat convection, and heat radiation. Compared with heat conduction and convection, the heat transfer of heat radiation is very small, so the influence of heat radiation is ignored.

(1) Heat conduction within a component [27]

For a single component, when heat conduction occurs within the component, the heat flow is

$$H_C = k_T A_S (T_1 - T_2) / L_D \tag{14}$$

where k_T is the thermal conductivity; T_1 and T_2 are the temperature of two points; A_S is the heat conduction area; L_D is the distance between these two points.

(2) Heat conduction between contact parts

For heat conduction between contact parts, the heat flow is

$$H_{CC} = TCC \cdot A_C (T_1 - T_2) \tag{15}$$

where TCC is the contact thermal conductivity at the contact; A_C is the contact area; T_1 and T_2 are the temperatures of the target node and the contact node, respectively.

(3) Surface heat convection of stationary parts

The bearing seat and outer ring are fixed, and the convective heat transfer coefficient can be calculated by the following formula:

$$h_v = \begin{cases} 0.53k_\alpha(Gr\mathrm{Pr})^{0.25}/L_D, & \text{Natural heat convection} \\ 0.3k_\alpha \mathrm{Re}^{0.57}/L_D, & \text{Forced heat convection} \end{cases} \quad (16)$$

where k_α is the thermal conductivity of air; Pr is the Prandtl number; Re is Reynolds number; L_D is the characteristic length; Gr is the Grashov number, $Gr = g\beta_V \Delta T {L^3}_D/v^2$, g is the gravitational acceleration, β_V is the coefficient of air volume expansion, and ΔT is the temperature difference; v is the kinematic viscosity of air.

(4) Surface heat convection of rotating parts

For the rotating inner ring and main shaft, the surface heat transfer coefficient is

$$h_v = \begin{cases} 0.4k_\alpha \mathrm{Re}^{0.5}\mathrm{Pr}^{0.33}/L_D, & \mathrm{Re} > 2.5 \times 10^5 \\ 0.0238k_\alpha \mathrm{Re}^{0.8}\mathrm{Pr}^{0.6}/L_D, & \mathrm{Re} > 3.2 \times 10^5 \end{cases} \quad (17)$$

For the rotating rollers, the surface heat transfer coefficient is

$$h_v = 0.33k_\alpha \mathrm{Re}^{0.5}\mathrm{Pr}^{0.4}/L_D \quad (18)$$

2.4. Simulation of Bearing Temperature

2.4.1. Finite Element Model

The test bearing is a railway freight car bearing 353130B, a double-row tapered roller bearing composed of a double raceway outer ring and two separating inner rings. Table 1 shows its main parameters. The bearing is modeled based on ABAQUS, and the steady-state temperature field of heat conduction is analyzed. Figure 5 shows the model. The total number of nodes is 1,167,669, and the total number of grids is 1,048,800.

Table 1. Structural parameters of railway bearing 353130B.

Model	Inner Ring Diameter (mm)	Outer Ring Diameter (mm)	Outer Ring Width (mm)	Effective Length of Roller (mm)	Roller Large End Diameter (mm)	Diameter of Small End of Roller (mm)	Number of Single Row Rollers
353130B	150	250	160	50	22.62	20.68	23

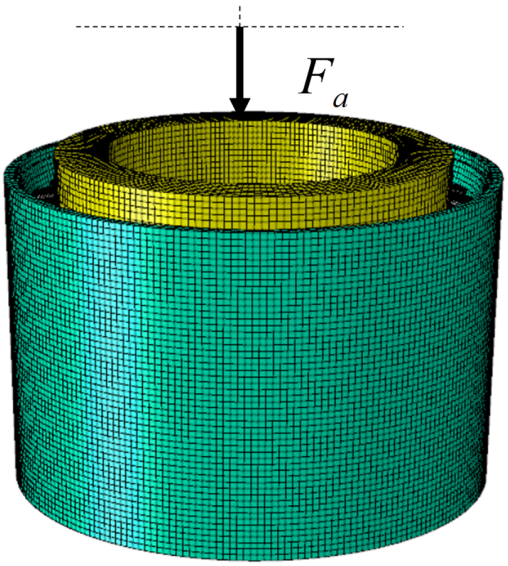

Figure 5. Finite element model.

2.4.2. Heat Flux Density Model

For the rotating roller and inner ring, the contact position between the roller and the raceway constantly changes; the contact position between the roller and the retaining edge also continually changes. The actual contact surface between the roller and the inner and outer ring is subjected to the action of a moving heat source. Therefore, the heat flux density between the roller and the inner ring raceway and between the roller and the inner ring retaining edge can be evenly distributed along the contact surface of the whole circumference, and the following formula can calculate the heat flux density.

$$q = \frac{\sum_{j=1}^{Z} H(j)}{S} \tag{19}$$

where $H(j)$ is the heat flow allocated to the roller contact surface or inner ring contact surface of the jth roller; S is the total heat generating area of the entire circumferential surface of the rotating surface.

The heat generated at every roller and raceway contact area is evenly distributed along the surface of the rollers and ferrule. The heat generated at every roller and retaining edge contact area is evenly distributed along the surface of the rollers and retaining edge. The viscous friction loss of grease is evenly distributed along the surface of the rollers, and the heat flow load is carried out on the model, as shown in Figure 6.

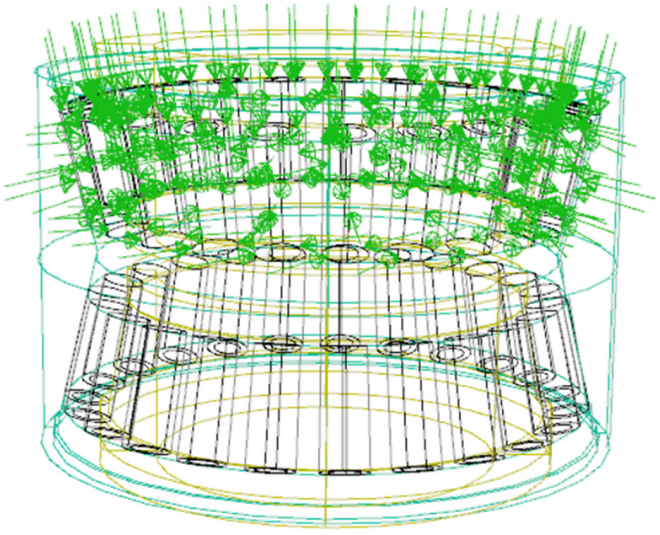

Figure 6. Heat flux density model.

3. Test Scheme

3.1. Sensor Selection

In this paper, the sensor is the self-developed adaptive thin-film thermocouple temperature sensor [26], as shown in Figure 7. When the train running speed is 360 km/h, the corresponding wheel speed is about 2220 r/min. After calculation, the time for the large end face of a single roller to pass through a fixed point is 1.6ms, and the dynamic response time of the sensor is 1.42 μs. It meets the requirements of roller temperature measurement. The set screw fixed the sensor on the sealing cover. The temperature measuring end of the sensor is a hemispherical body with a diameter of 5 mm, which is in contact with the large end face of the roller during temperature measurement. We set the sensor mounting position as shown in Figure 8.

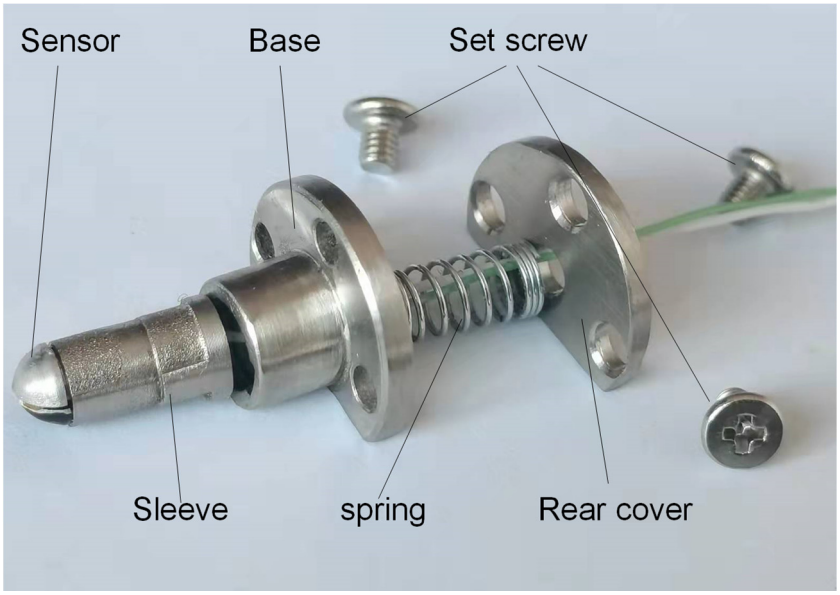

Figure 7. Adaptive thin-film temperature sensor.

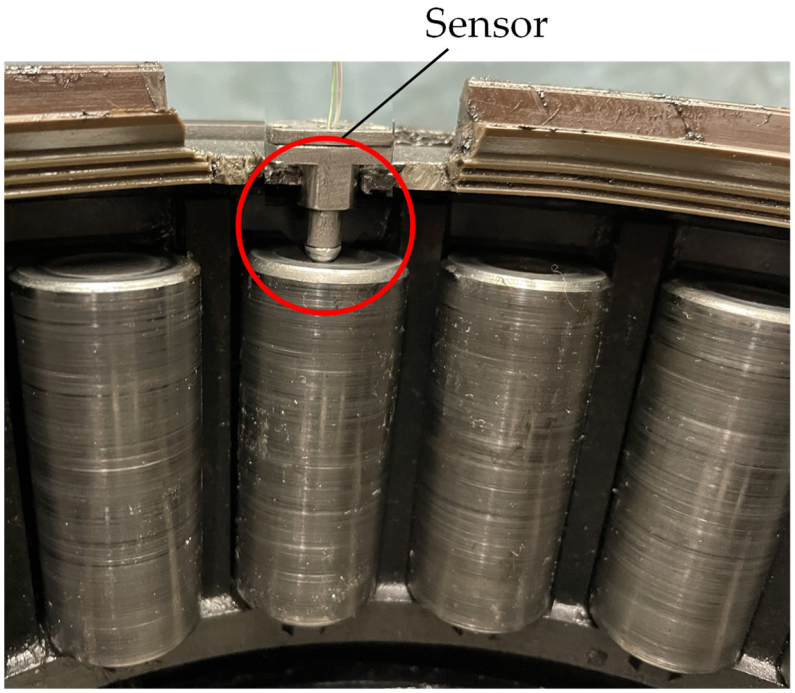

Figure 8. Sensor mounting position.

3.2. Temperature Measuring Point

To obtain the temperature distribution characteristics and influence law of the test bearing, we evenly arranged three temperature measuring points on the outer surface of the outer ring. Three measuring points are evenly arranged on the circumference of the sealing cover to measure the roller temperature. We evenly set three temperature measuring points on the rim of the inner ring. Figure 9a shows the specific location. Three temperature measuring points are evenly placed on the outer surface of the outer ring of the first row of bearings to measure the axial temperature distribution of the bearings, as shown in Figure 9b.

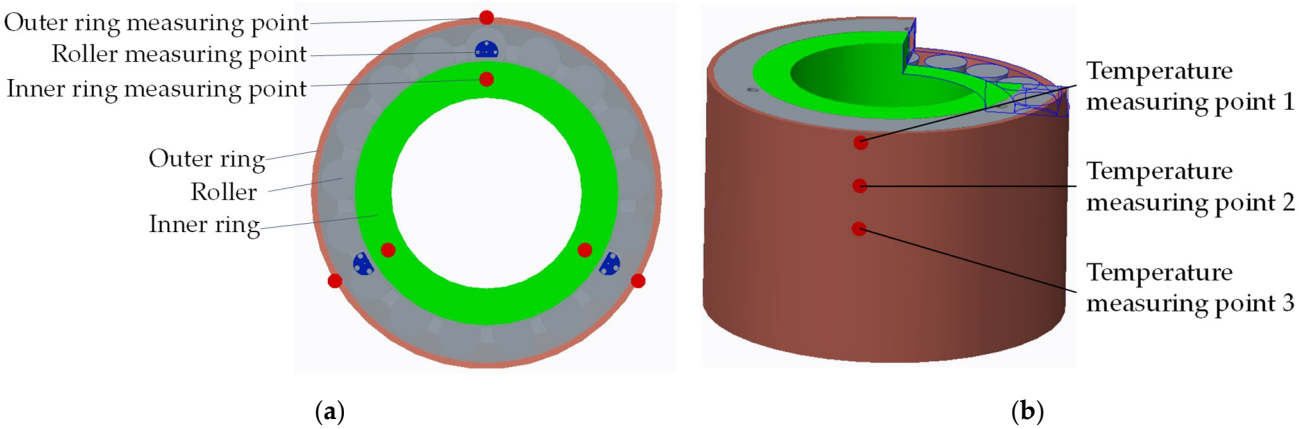

Figure 9. Location of temperature measuring point of railway bearing: (**a**) circumferential temperature measuring point; (**b**) axial temperature measuring point of outer ring.

When the bearing is running, the outer ring is fixed, and the temperature of the outer ring temperature measuring point can be measured directly by the infrared temperature measuring gun. We obtained the average roller temperature by using the self-developed adaptive thin-film temperature sensor. We fixed the infrared temperature measuring gun on the test bench, adjusted the angle to align it with the outer surface of the inner ring retaining edge; the inner ring rotated stably and the position of the infrared temperature measuring gun remained unchanged. We then estimated the average temperature of the inner ring.

3.3. Test Rig Assembly

The railway bearing thermal analysis test-bed is shown in Figure 10, which mainly includes the bearing dynamic quality detection test machine [28], mechanical system control box, digital multimeter, and adaptive thin-film thermocouple temperature sensor.

Figure 10. Railway bearing thermal analysis test bench.

A vertical telescopic axial loading system for the mechanical test-bed comprises an axial loading mechanism, lifting workbench, spindle rotation mechanism, and railway bearing. The upper row is the first column, and the lower row is the second column.

The specific workflow includes the following steps: start the measurement program, and the loading cylinder will push the loading disc upward. When the loading disc contacts the end face of the bearing outer ring, the bearing outer ring begins to move upward. Under the action of gravity, the second row of bearing (inner ring, rolling element, and retainer)

and the intermediate spacer will sag freely and separate from the outer ring. The loading disc continues to push the bearing upward until the mandrel is fully matched with the inner ring of the first row of the bearing, as shown in Figure 11. Set the spindle speed and continue the program. The motor drives the spindle to rotate. After one measurement, the loading cylinder drops, returns the bearing to its original position, manually turns over the tested bearing, repeats the above process, and measures the bearing on the other side.

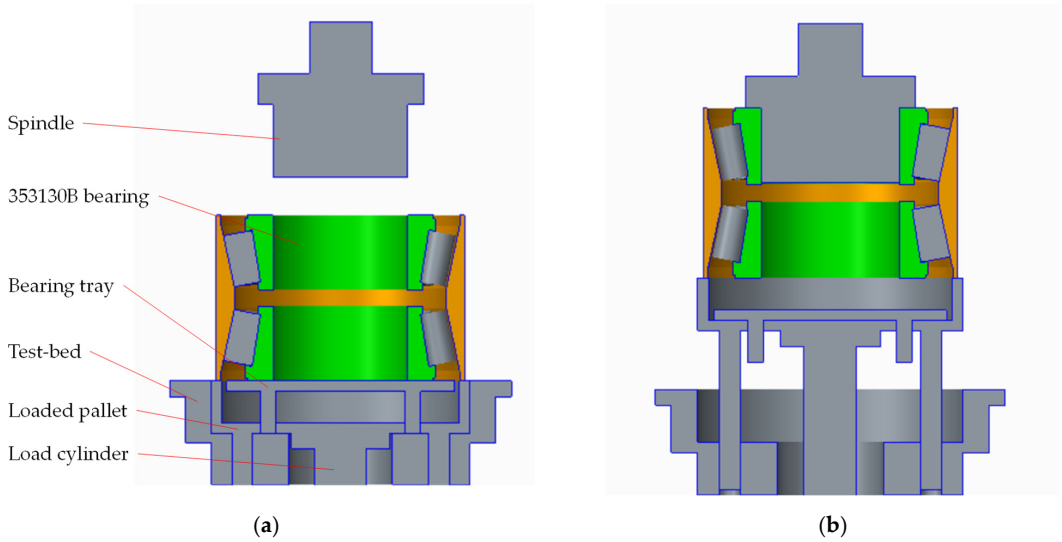

Figure 11. Test bench structure: (**a**) initial location map; (**b**) location map during measurement.

4. Results and Discussion

4.1. Comparative Temperature Measurement

To improve the accuracy of the measurement results, before the temperature measurement test of the bearing, the temperature measurement comparison test is carried out between the infrared temperature gun and the thin-film thermocouple sensor. We closed and fixed the measuring end of the thin-film sensor on the outer surface of the bearing outer ring, and fixed the infrared temperature measuring gun so that its temperature measuring point was located on the same contour line as that of the thin-film temperature sensor, as shown in Figure 12a. We set the spindle speed to 1000 rpm for the temperature measurement comparison test.

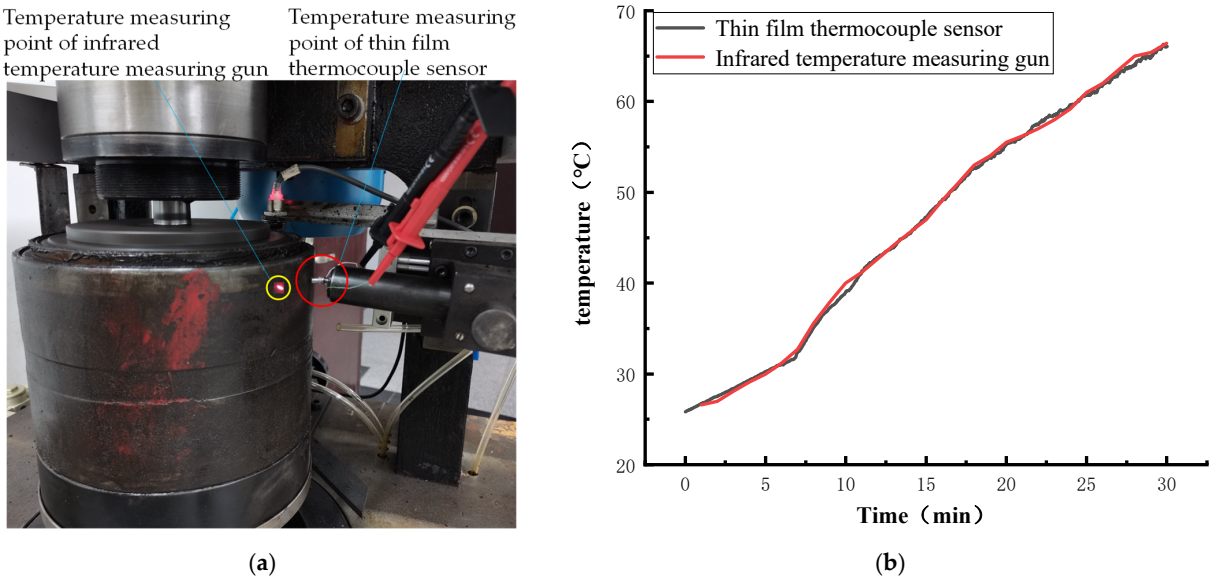

Figure 12. Comparative temperature measurement test: (**a**) location of temperature measuring point; (**b**) temperature comparison diagram.

Figure 12b shows the comparison results. The results show that the maximum temperature difference measured by the two methods is about 1 °C, and the error is acceptable.

4.2. Stress Distribution

4.2.1. Influence of Axial Load

The spindle speed is 800 rpm, and the axial load is 600 N, 1200 N, 1800 N, 2400 N, and 3000 N, respectively. We calculated the change in contact load inside the bearing, as shown in Figure 13. The results show that the contact load inside the bearing increases linearly with the increase in axial load, which is mainly reflected in the rise in contact load between the inner and outer race raceways and rollers.

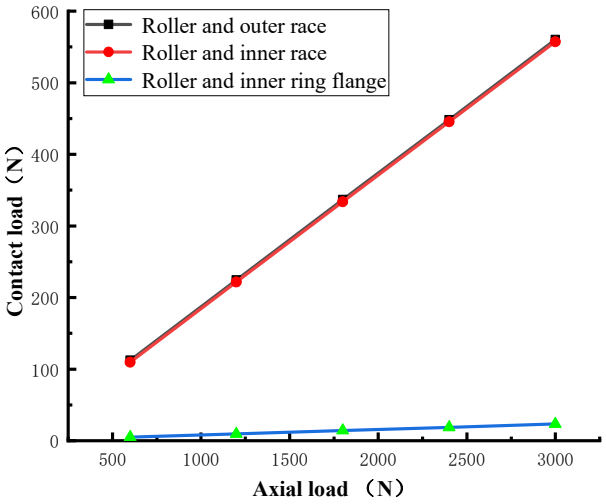

Figure 13. Influence of axial load.

4.2.2. Influence of Speed

The axial load is 3000 N, and the spindle speed is 600 rpm, 1200 rpm, 1800 rpm, 2400 rpm, and 3000 rpm, respectively. We calculated the change in contact load inside the bearing, as shown in Figure 14. The results show that with the increase in spindle speed, the contact load between the outer ring and the roller and the contact load between the large flange of the inner ring and the roller gradually increases. In contrast, the contact load between the inner ring and the roller decreases gradually because the centrifugal force of the roller increases gradually with the increase in rotating speed, to reduce the pressure of the roller on the inner ring.

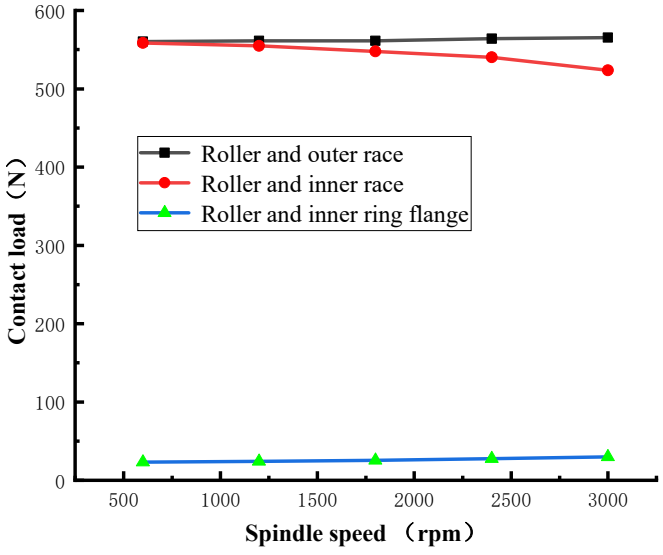

Figure 14. Influence of speed.

4.3. Simulation of Temperature Distribution

The simulation results under the given operating conditions (rotating speed is 800 rpm, the radial load is 0 N, the axial load is 2400 N) are shown in Figure 15.

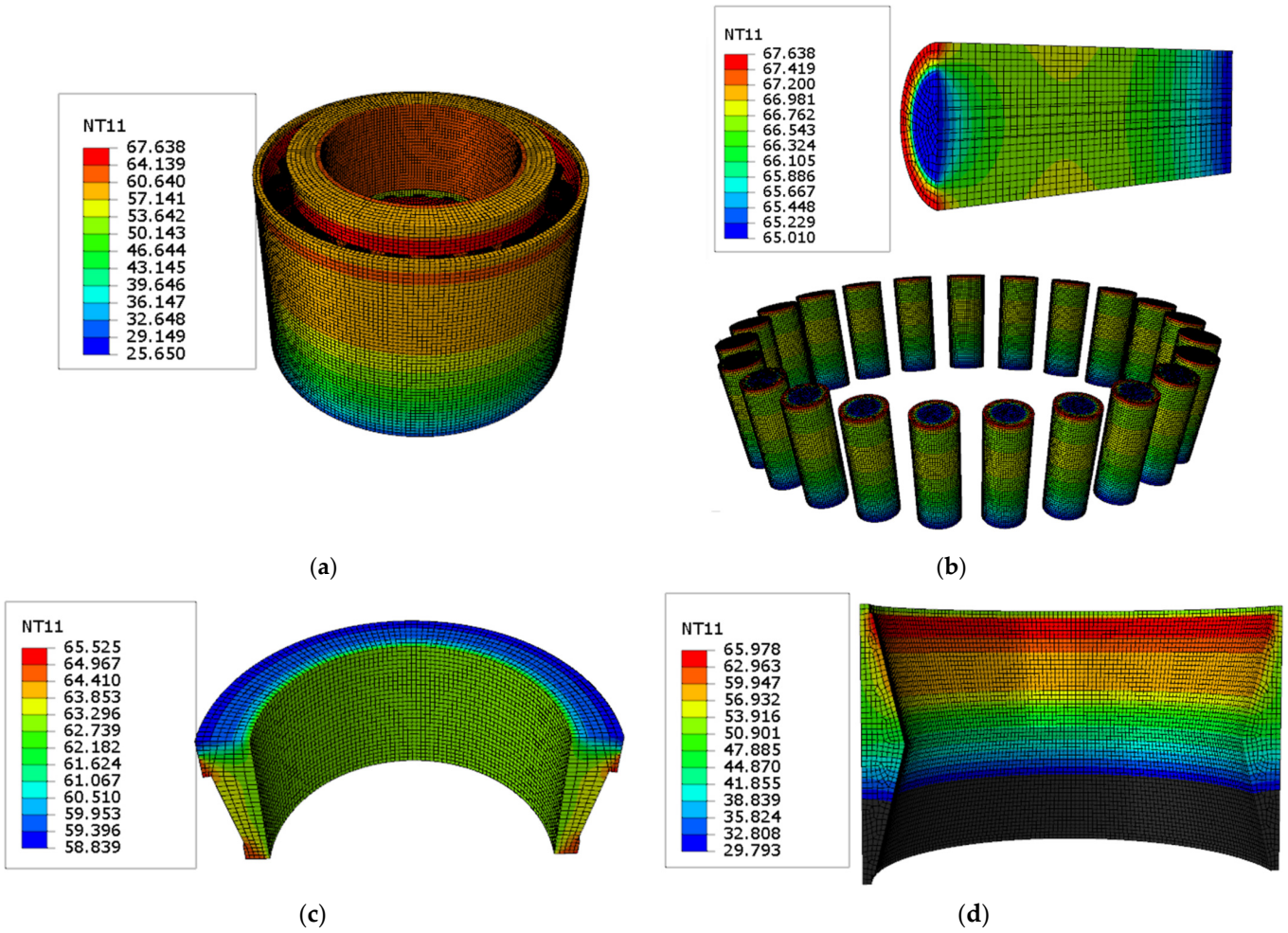

Figure 15. Temperature field simulation of railway wagon bearing 353130B: (**a**) bearing; (**b**) roller; (**c**) inner ring; (**d**) outer ring.

As shown in Figure 15, the maximum temperature of the bearing is located on the contact surface between the roller and the large retaining edge of the inner ring. The circumferential temperature of the bearing is evenly distributed. As shown in Table 2, the test results are higher than the simulation results. Although there are errors, the test results and simulation results have the same trend in temperature rise and temperature distribution, and the maximum error is within 15%, which is acceptable in engineering.

Table 2. Comparison between simulation results and experimental data.

Temperature Measuring Position		Simulation Temperature (°C)	Test Temperature (°C)	Temperature Difference (°C)	Error (%)
Inner ring		59.69	65.55	5.86	8.94
Roller		67.08	72.02	4.94	6.86
Outer ring	Temperature measuring point 1	62.22	65.37	3.15	4.82
	Temperature measuring point 2	60.14	64.67	4.53	7.01
	Temperature measuring point 3	58.70	59.01	0.31	0.52

4.4. Temperature Rise

Figure 16 shows the temperature rise curve of each temperature measuring point of railway bearing from the start to temperature stability under working conditions (rotating speed is 800 rpm, the radial load is 0 N; the axial load is 2400 N).

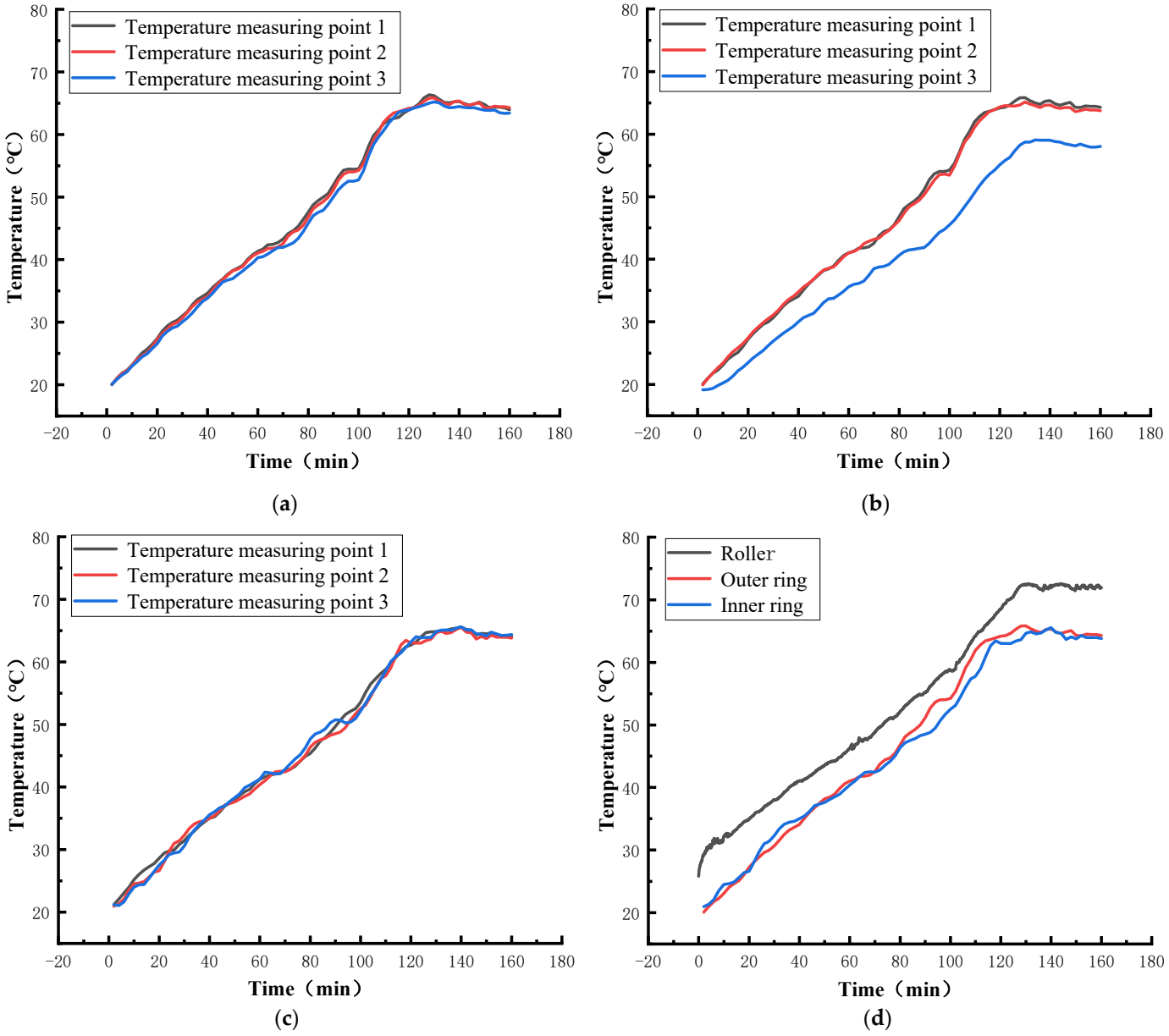

Figure 16. Temperature rise curve of railway bearing 353130B: (**a**) the circumferential direction of outer ring; (**b**) outer ring axial; (**c**) the circumferential direction of inner ring; (**d**) radial bearing.

As shown in Figure 16, the circumferential temperature distribution of railway bearing is uniform. The temperature rise characteristics of the axial temperature measuring point of the outer ring are slightly different, and the temperature of temperature measuring point 3 is low because the temperature measuring point 3 is far away from the bearing heat source and has good heat dissipation. Figure 16d shows that the inner ring, roller, and outer ring have different temperature rise characteristics during operation. After the temperature is stable, the roller temperature is higher than that of the inner and outer rings. The stable temperature of the roller is 72.02 °C, the stable temperature of the inner ring is 65.55 °C, and the stable temperature of the outer ring is 64.67 °C. It is caused by heat loss in the process of heat conduction.

4.5. Effect of Rotating Speed on Temperature Distribution

When studying the influence of the spindle speed on temperature rise and temperature distribution, one must keep the radial load of 0 N, the axial load of 2400 N must be unchanged, and one must measure the steady-state temperature of the bearing at different speeds.

Figure 17 shows the temperature rise of the bearing inner ring, roller, and outer ring at different speeds. With the increase in rotating speed, the temperature of the inner ring, roller, and outer ring also increases rapidly. The average temperature of the roller is higher than that of the inner ring. The average temperature of the inner ring is higher than that of the outer ring (see Figure 17d). The rotating speed increases from 200 rpm to 800 rpm. The temperature of the roller increases from 28.2 °C to 46 °C. The temperature of the outer ring increases from 25.1 °C to 43.9 °C. The temperature of the inner ring increases from 27.2 °C to 44.7 °C. Therefore, the temperature rise of the outer ring changes the most (18.8 °C), followed by the roller (17.8 °C), and the temperature rise of the inner ring changes the least (17.5 °C). As shown in Figure 17d, the temperature rise rate decreases when the speed is higher than 600 rpm. Because with the increase in temperature, the viscosity of grease becomes lower, the lubrication performance is improved and the viscous friction loss and the heat production are reduced.

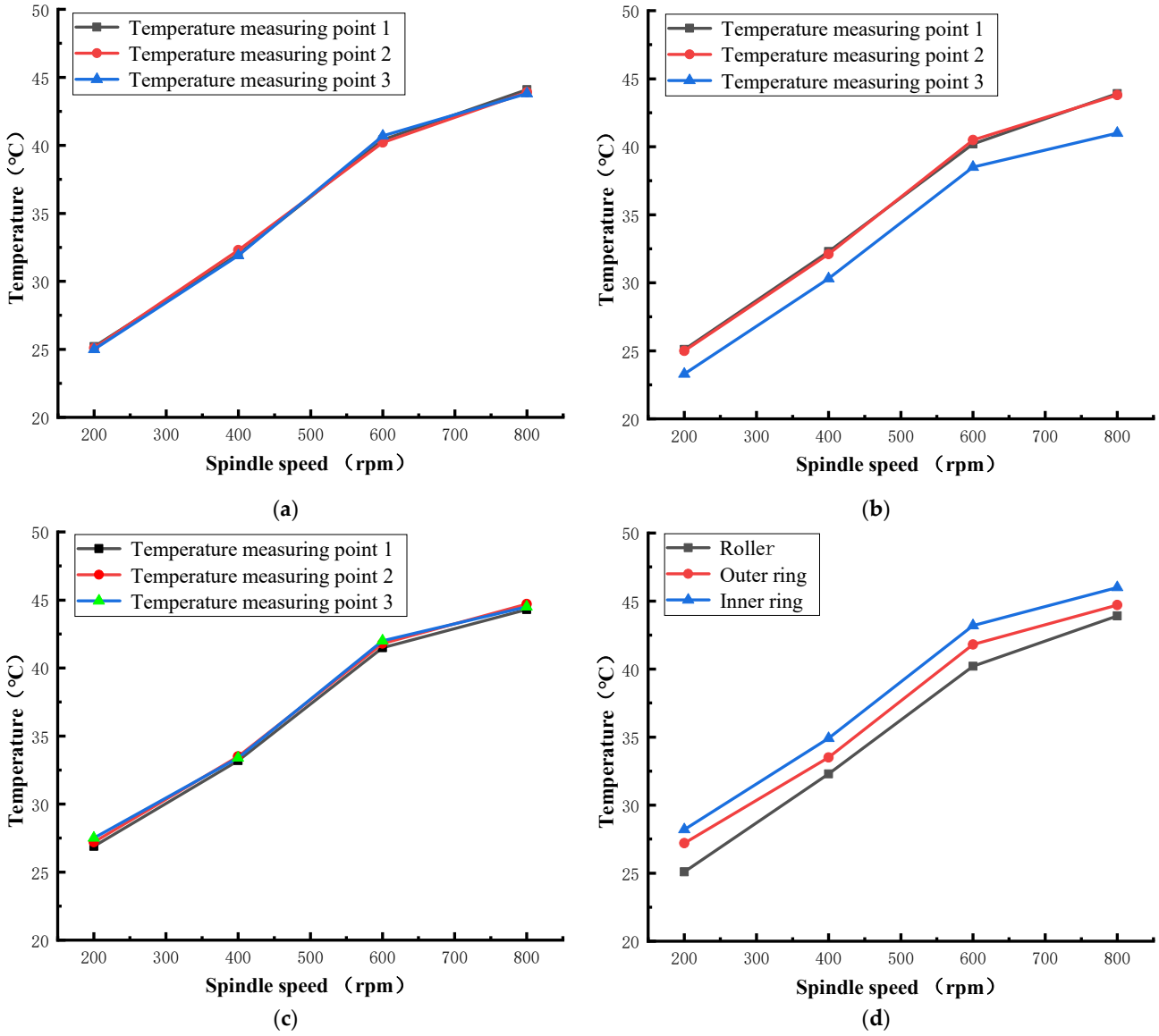

Figure 17. Temperature rise of railway bearing 353130B at different speeds: (**a**) circumferential direction of outer ring; (**b**) outer ring axial; (**c**) circumferential direction of inner ring; (**d**) radial bearing.

5. Conclusions

(1) We established the quasi-static mechanical model according to the test conditions, and obtained the contact load distribution and kinematic parameters of railway double-row tapered roller bearing. We obtained the steady-state temperature field of the test bearing 353130B through finite element analysis, which is consistent with the test results. The influence of different axial loads and rotating speed on bearing load distribution was analyzed, and then the impact on bearing temperature distribution was obtained.

(2) We built a bearing testbed to measure the temperature of the inner ring, roller, and outer ring of a railway freight car bearing 353130B. We obtained the stable temperature and the distribution of the bearing at different speeds.

(3) The spindle speed mainly affects the bearing temperature rise rate and has little effect on the temperature distribution. Compared with the stable temperature gradually rising from 200 rpm to 800 rpm, the former has a faster temperature rise rate and a higher final stable temperature.

However, much remains to be done, such as high-speed railway bearing experiments, actual locomotive experiments, bearing temperature curve prediction models, temperature measurement tests of faulty bearing and fault prediction, etc. Through constant research, new ideas are being researched on bearing fault diagnosis. A reference is provided for enhancing the temperature monitoring system of a train bearing to provide a safety guarantee for the train speed increase.

Author Contributions: Conceptualization, G.M. and P.G.; methodology, W.T.; investigation, P.G.; data curation, Y.W. and P.G.; writing—original draft preparation, P.G.; writing—review and editing, Y.C. and J.Y. All authors have read and agreed to the published version of the manuscript.

Funding: This research was funded by the National Natural Science Foundation of China (52175379, 51905071), the Doctoral Research Foundation of Liaoning Province (2019-BS-043), the Key Laboratory of Precision and Special Processing of Ministry of Education, and the Dalian University of Technology (JMTZ201902).

Informed Consent Statement: Informed consent was obtained from all subjects involved in the study.

Data Availability Statement: Data in this paper are available from the corresponding authors upon request.

Conflicts of Interest: The authors declare no conflict of interest. The funders had no role in the design of the study; in the collection, analyses, or interpretation of data; in the writing of the manuscript; or in the decision to publish the results.

References

1. Chang, Z.; Jia, Q.; Yuan, X.; Chen, Y. Main failure mode of oil-air lubricated rolling bearing installed in high speed machining. *Tribol. Int.* **2017**, *112*, 68–74. [CrossRef]
2. Nikas, G.K. An Advanced Model to Study the Possible Thermomechanical Damage of Lubricated Sliding-Rolling Line Contacts from Soft Particles. *J. Tribol.* **2001**, *123*, 828–841. [CrossRef]
3. Sun, Q.G.; Wang, Y.F.; Wang, Y.; Lv, H.B. Comparing of Temperatures of Rolling Bearing under the Oil-Air Lubrication to the Spray Lubrication. *Appl. Mech. Mater.* **2013**, *395–396*, 763–768. [CrossRef]
4. Hamraoui, M. Thermal behaviour of rollers during the rolling process. *Appl. Therm. Eng.* **2009**, *29*, 2386–2390. [CrossRef]
5. Takabi, J.; Khonsari, M.M. On the thermally-induced seizure in bearings: A review. *Tribol. Int.* **2015**, *91*, 118–130. [CrossRef]
6. Winer, W.O.; Bair, S.; Gecim, B. Thermal resistance of a tapered roller bearing. *Tribol. Trans.* **1986**, *29*, 539–547. [CrossRef]
7. Hoeprich, M. Rolling-Element Bearing Internal Temperatures. *Tribol. Trans.* **1996**, *39*, 855–858. [CrossRef]
8. Craig, M.; Harvey, T.J.; Wood, R.J.K.; Masuda, K.; Kawabata, M.; Powrie, H.E.G. Advanced condition monitoring of tapered roller bearings, Part 1. *Tribol. Int.* **2009**, *42*, 1846–1856. [CrossRef]
9. Takabi, J.; Khonsari, M.M. Experimental testing and thermal analysis of ball bearings. *Tribol. Int.* **2013**, *60*, 93–103. [CrossRef]
10. Jeng, Y.R.; Gao, C.C. Investigation of the ball-bearing temperature rise under an oil-air lubrication system. *Proc. Inst. Mech. Eng. Part J J. Eng. Tribol.* **2001**, *215*, 139–148. [CrossRef]
11. Jiang, S.; Mao, H. Investigation of the High Speed Rolling Bearing Temperature Rise with Oil-Air Lubrication. *J. Tribol.* **2011**, *133*, 655–664. [CrossRef]

12. Li, Z.; Ma, H.; Guo, F.; Li, X.; Liu, M. Experimental Research on Oil- Air Lubrication for Tapered Roller Bearings. *Bearing* **2016**, *8*, 42–45.
13. Scott, S.; Kovacs, A.; Gupta, L.; Katz, J.; Sadeghi, F.; Peroulis, D. Wireless temperature microsensors integrated on bearings for health monitoring applications. In Proceedings of the 2011 IEEE 24th International Conference on Micro Electro Mechanical Systems, Cancun, Mexico, 23–27 January 2011; pp. 660–663.
14. Tarawneh, C.M.; Fuentes, A.A.; Kypuros, J.A.; Navarro, L.A.; Vaipan, A.G.; Wilson, B.M. Thermal Modeling of a Railroad Tapered-Roller Bearing Using Finite Element Analysis. *J. Therm. Sci. Eng. Appl.* **2012**, *4*, 031002. [CrossRef]
15. Tarawneh, C.M.; Cole, K.D.; Wilson, B.M.; Alnaimat, F. Experiments and models for the thermal response of railroad tapered-roller bearings. *Int. J. Heat Mass Transf.* **2008**, *51*, 5794–5803. [CrossRef]
16. Flouros, M.; Stadlbauer, M.; Cottier, F.; Proestler, S.; Beichl, S. Transient Temperature Measurements in the Contact Zone Between Brush Seals of Kevlar and Metallic Type for Bearing Chamber Sealing Using a Pyrometric Technique. In *Turbo Expo: Power for Land, Sea, and Air*; American Society of Mechanical Engineers: New York, NY, USA, 2012; Volume 44670, pp. 73–80.
17. Dong, Y.; Zhou, Z.; Liu, Z.; Zheng, K. Temperature field measurement of spindle ball bearing under radial force based on fiber Bragg grating sensors. *Adv. Mech. Eng.* **2015**, *7*, 1687814015620332. [CrossRef]
18. Liu, M.; Zhou, W.; Song, H.; Dong, Y.; Wang, W.; Zhou, S. Study of the temperature distribution of a machine tool spindle bearing based on FBG quasi-distributed sensing. *Int. J. Adv. Manuf. Technol.* **2018**, *98*, 263–274. [CrossRef]
19. Henao-Sepulveda, J.A.; Toledo-Quiñones, M.; Jia, Y. Contactless Monitoring of Ball Bearing Temperature. In Proceedings of the Instrumentation and Measurement Technology Conference, Taipei, Taiwan, 16–19 May 2005.
20. Brecher, C.; Fey, M.; Hassis, A.; Bonerz, S. High-Speed Rolling Bearing Test Rigs with Contactless Signal Transmission for Measuring the Inner Ring Temperature. In Proceedings of the European Telemetry and Test Conference, Nürnberg, Germany, 3–5 June 2014.
21. Zhou, X.; Zhang, H.; Hao, X.; Liao, X.; Han, Q. Investigation on thermal behavior and temperature distribution of bearing inner and outer rings. *Tribol. Int.* **2018**, *130*, 289–298. [CrossRef]
22. Zhou, X.; Zhu, Q.; Wen, B.; Zhao, G.; Han, Q. Experimental Investigation on Temperature Field of a Double-Row Tapered Roller Bearing. *Tribol. Trans.* **2019**, *62*, 1086–1098. [CrossRef]
23. Yan, K.; Gao, C.; Zhu, Y.S.; Hong, J. Research Technology the Temperature Measurement Principle and Realization Rolling Bearing Inner Ring Based on CdTe Quantum Dots. *J. Mech. Eng.* **2017**, *53*, 134–140. [CrossRef]
24. Yan, K.; Yan, B.; Li, B.Q.; Hong, J. Investigation of bearing inner ring-cage thermal characteristics based on CdTe quantum dots fluorescence thermometry. *Appl. Therm. Eng.* **2017**, *114*, 279–286. [CrossRef]
25. Zhang, P.; Yan, K.; Pan, A.; Zhu, Y.; Hong, J.; Liang, P. Use of CdTe Quantum Dots as Heat Resistant Temperature Sensor for Bearing Rotating Elements Monitoring. *IEEE J. Sel. Areas Commun.* **2020**, *38*, 463–470. [CrossRef]
26. Cui, Y.; Gao, P.; Tang, W.; Mo, G.; Yin, J. Adaptive Thin-film Temperature Sensor for Bearing's Rolling Elements Temperature Measurement. *Sensors* **2022**, *22*, 2838. [CrossRef] [PubMed]
27. SKF. Rolling Bearings. 2017. Available online: http://www.skf.com/binary/30-121486/10000_3-EN-webb.pdf (accessed on 1 May 2021).
28. Zhang, Y.N.; Tang, W.C.; Xu, W.; Xu, S.N. Automatic Dynamic Quality Inspection System and Method for Vertical Double-row Tapered Roller Bearing. Chinese Patent CN111323229A, 23 June 2020.